Supplementary Information

Composition Sensitive Selectivity and Activity of Carbon Dioxide Electroreduction on Pd-Cu Solid-Solution Alloy Nanoparticles

Naoto Todoroki[1], Masanao Ishijima[2*] Jhon L. Cuya Huaman[1], Yuto Tanaka[3] and Jeyadevan Balachandran[1]*

[1]Graduate School of Environmental Studies, Tohoku University, 6-2-2 Aramakiaza-Aoba Aoba-ku, Sendai 980-8579, Japan

[2]Department of Applied Chemistry for Environment, Tokyo Metropolitan University, 1-1 Minamiosawa, Hachioji, Tokyo 192-0397, Japan

[3] Department of Materials Science, The University of Shiga Prefecture, Hikone, Shiga 522-8533, Japan

*Corresponding Author

E-mail: naoto.todoroki.b1@tohoku.ac.jp

E-mail: ishijima@tmu.ac.jp

1. Summary of faradaic efficiencies of Pd-Cu alloy, pure Pd, and Cu NPs

Faradaic efficiencies (FEs) for all CO_2RR products of Pd-Cu alloy, pure Pd, and Cu NPs are summarized in Fig.S1. The FEs for hydrocarbons (CH_4 and C_2H_4) are very small on all the Pd-Cu alloy and pure Pd NPs. In contrast, pure Cu NPs show selectivity for the hydrocarbons and alcohols at low potential regions (< −0.97 V vs RHE), as previously reported [1].

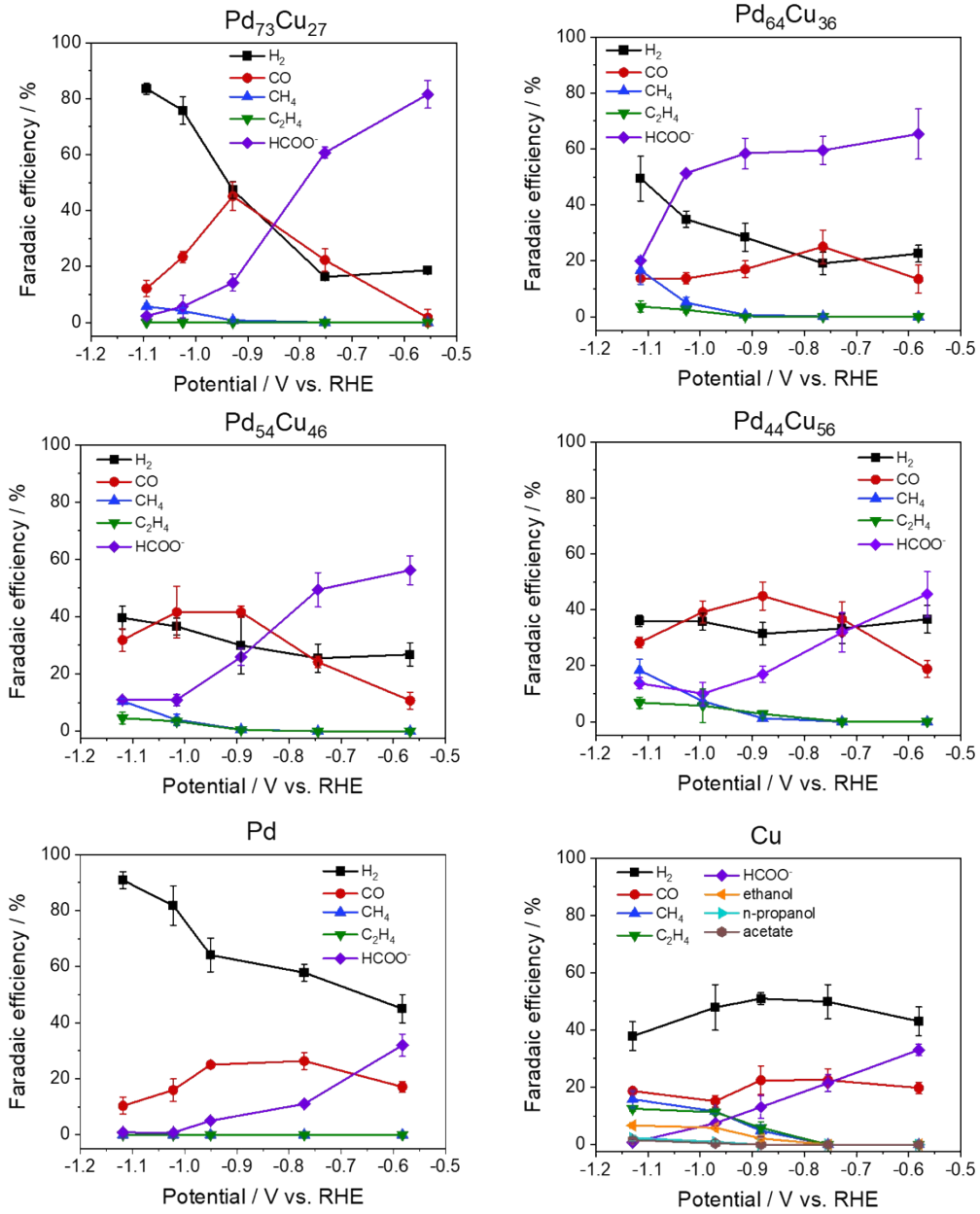

Fig.S1 Faradaic efficiency for CO_2RR products of Pd-Cu alloy, pure Pd and Cu nanoparticles

2. Partial current density for CH_4 and C_2H_4

Partial current densities for CH_4 and C_2H_4 are shown in Fig.S2. Both the current densities increase with increasing the Cu composition in Pd-Cu alloy NPs. The highest values are achieved with pure Cu NPs for CH_4 and C_2H_4.

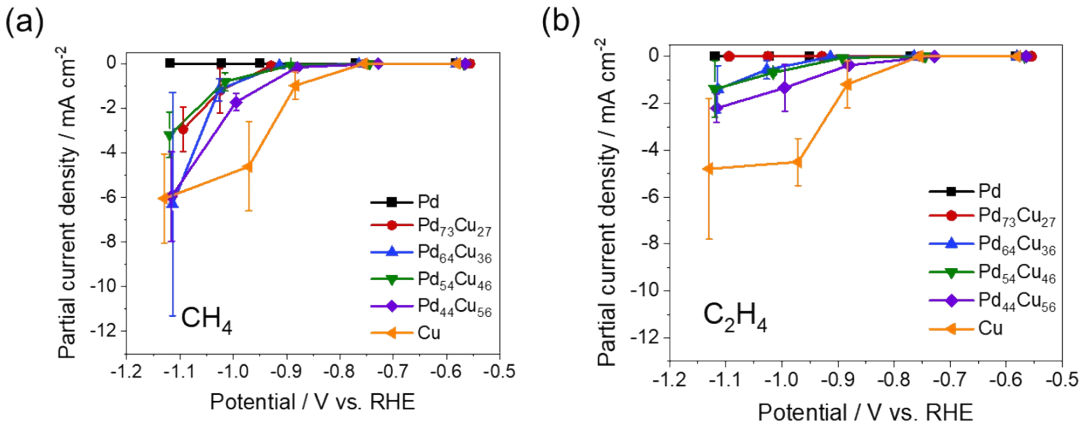

Fig.S2 Partial current densities for (a) CH_4 and (b) C_2H_4.

3. Linear sweep voltammograms and cyclic voltammograms

Fig.S3(a) and (b) are linear sweep voltammograms (LSV) and cyclic voltammograms (CV) recorded in CO_2-saturated 0.5 M $KHCO_3$ solution after constant potential electrolysis for CO_2RR properties evaluation. As for the LSV (a), $Pd_{44}Cu_{56}$, $Pd_{54}Cu_{46}$, $Pd_{64}Cu_{36,}$ and pure Cu NPs show lower onset potential for CO_2RR than $Pd_{73}Cu_{27}$ and pure Pd NPs. The abrupt increase in current density from −0.9 V for $Pd_{73}Cu_{27}$ and pure Pd NPs is probably derived from selective hydrogen evolution (Fig 4 in the main manuscript). The CV curves show redox features corresponding to the oxidation-reduction reaction of the Cu surface of Pd-Cu alloy NPs increasing with the Cu composition, indicating that the Cu surface composition increases. We can't evaluate the electrochemical surface areas from the CV measurement because there are no common potential windows without faradaic reactions for Pd-Cu alloy NPs. However, judging from the double layer capacitance regions (0.4-0.6 V) in the CV curves (b), we assume that there is no significant difference in the electrochemical surface areas.

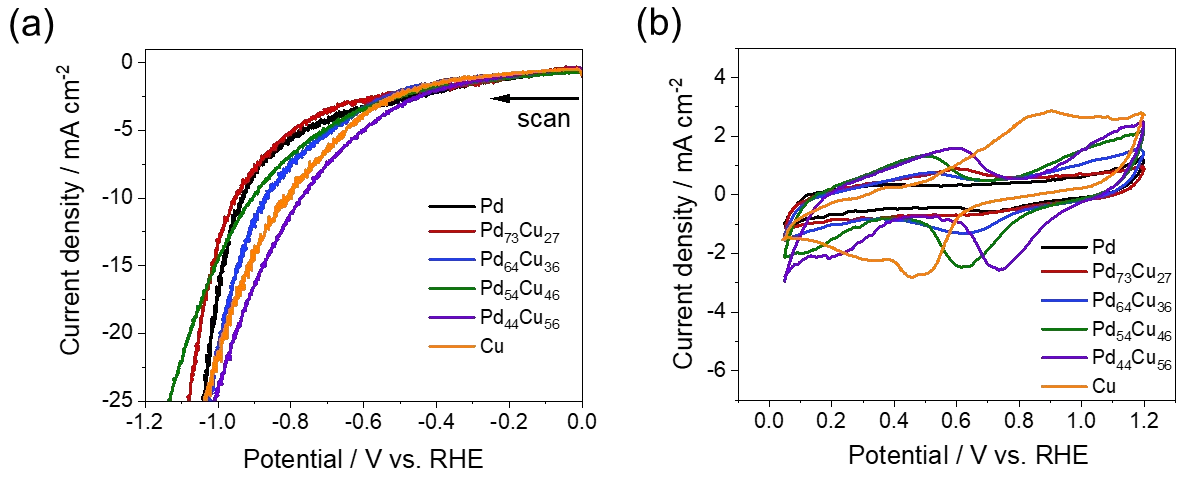

Fig.S3 (a) Linear sweep voltammograms recorded in CO_2-saturated 0.5 M $KHCO_3$ at a scan rate of 5 mV s^{-1}. (b) Cyclic voltammograms were recorded in CO_2-saturated 0.5 M $KHCO_3$ at a scan rate of 50 mV s^{-1}.

4. XRD patterns of pure Cu and Pd NPs

Fig.S4 shows XRD patterns of pure Cu and Pd nanoparticles. The estimated crystallite sizes of Cu and Pd estimated from Scherrer equation were 31.2 and 1.85 nm, respectively.

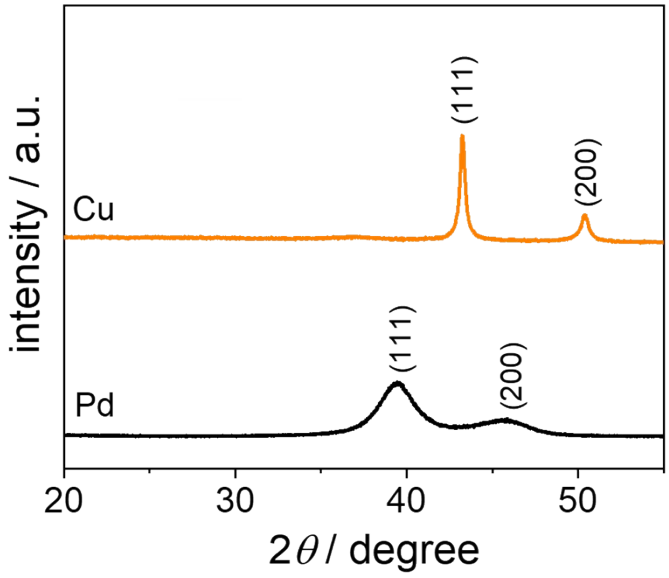

Fig.S4 XRD patterns of pure Cu and Pd nanoparticles.

5. Comparison of CO_2RR properties of Pd-Cu NPs with previous reports

Table S1. Comparison of faradaic efficiency and partial current density for formate and CO of Pd-Cu alloy NPs evaluated in this study with previous reports.

Alloy composition	Structure	Electrolyte	Formate				CO				Ref.
			FE		Partial current density (PCD)		FE		Partial current density (PCD)		
			FE / %	Potential vs. RHE / V	PCD / mA cm^{-2}	Potential vs. RHE / V	FE / %	Potential vs. RHE / V	PCD / mA cm^{-2}	Potential vs. RHE / V	
$Pd_{82}Cu_{18}$	nano dendric architectures	0.1 M $KHCO_3$	96.0	-0.3	9.7	-0.8	4	-0.8	-	-	2
$Pd_{75}Cu_{25}$	nanodendrite	0.1 M $KHCO_3$	96.0	-0.31	6.4	-0.4	0	-	-	-	3
Pd_5Cu_1	NPs on Vulcan XC-72	0.5 M $NaHCO_3$	69.0	-0.15	-	-	0	-	-	-	4
Pd_3Cu	NPs on Vulcan XC-72R	0.1 M $KHCO_3$	0	-	-	-	87	-0.9	0.61	-1.1	5
$Pd_{85}Cu_{15}$	NPs on Vulkan XC-72R	0.1 M $KHCO_3$	1.6	-0.89	-	-	85	-0.9	14	-1.2	6
Pd_7Cu_3	Mesoporous structures	0.1 M KHCO3	-	-	-	-	79	-0.8	-	-	7
$Pd_{73}Cu_{27}$	NPs on GDL	0.5 M $KHCO_3$	81.5	-0.56	6.11	-0.56	44.9	-0.93	6.91	-1	This Study
$Pd_{64}Cu_{38}$			65.4	-0.58	11.8	-1.0	25.0	-0.76	5.2	-1.1	
$Pd_{54}Cu_{48}$			56.2	-0.57	3.31	-1.10	41.6	-0.89	9.68	-1.1	
$Pd_{44}Cu_{56}$			45.6	-0.56	4.44	-1.1	45.1	-0.88	9.2	-1.0	
Pd			32.0	-0.58	1.06	-0.58	26.3	-0.77	5.47	-1.1	
Cu			33.1	-0.58	2.96	-0.97	22.5	-0.88	7.15	-1.1	

References

1. Q. Li, W. Zhu, J. Fu, H. Zhang, G. Wu and S. Sun, *Nano Energy*, 2016, **24**, 1-9.
2. Y. Sun, F. Wang, F. Liu, S. Zhang, S. Zhao, J. Chen, Y. Huang, X. Liu, Y. Wu and Y. Chen, *ACS Appl. Mater.*, 2022, **14**, 8896-8905.
3. R. Zhou, X. Fan, X. Ke, J. Xu, X. Zhao, L. Jia, B. Pan, N. Han, L. Li, X. Liu, J. Luo, H. Lin and Y. Li, *Nano Lett.*, 2021, **21**, 4092-4098.
4. T. Takashima, T. Suzuki and H. Irie, *Electrochemistry*, 2019, **87**, 134-138.
5. Y. Mun, S. Lee, A. Cho, S. Kim, J. W. Han and J. Lee, *Appl. Catal., B*, 2019, **246**, 82-88.
6. Z. Yin, D. Gao, S. Yao, B. Zhao, F. Cai, L. Lin, P. Tang, P. Zhai, G. Wang, D. Ma and X. Bao, *Nano Energy*, 2016, **27**, 35-43.
7. M. Li, J. Wang, P. Li, K. Chang, C. Li, T. Wang, B. Jiang, H. Zhang, H. Liu, Y. Yamauchi, N. Umezawa and J. Ye, *J. Mater. Chem. A*, 2016, **4**, 4776-4782.